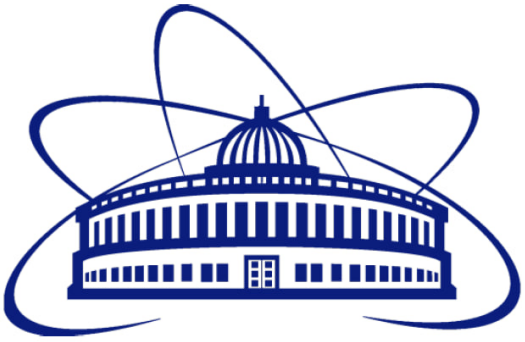

Joint Institute For Nuclear Research
Flerov Laboratory of Nuclear Reactions (FLNR)

Final Report on the INTEREST Programme
INTErnational REmote STudent Training Programme
(Wave 11, 5 November - 14 December, 2024)

PROMPT GAMMA RAY SPECTROSCOPY USING SEGMENTED HIGH PURITY GERMANIUM (HPGE) DETECTORS

Supervisor:
Dr.Aniruddha Dey

Student:
Kholmatova Odina
National University of Uzbekistan named after Mirzo Ulugbek (NUUz)
Tashkent, Uzbekistan

Dubna, 2024

Contents

Acknowledgements

I would like to extend my heartfelt gratitude to the INTEREST team for providing me with the incredible opportunity to join such a fascinating scientific project. This experience has deepened my insights and equipped me with valuable skills crucial for my growth as a young researcher.

At the beginning of the project, I started by noting down basic commands of the RADWARE software under the guidance of Dr. Aniruddha Dey. He explained various operations such as opening folders, managing files (renaming, copying, and removing), running programs, installing packages, and more. To help me better understand the material, I recorded our classes as voice messages. After each lesson, I would listen to the recordings, take notes on key points, and ask Dr. Dey for clarifications when needed. I then reviewed these notes thoroughly to ensure I could apply the concepts effectively.

Dr. Dey's lessons were exceptionally detailed. During each class, he walked us through every aspect of his presentation, ensuring we understood the material thoroughly. Before the lessons, he provided us with the study material, which I translated and reviewed in advance to familiarize myself with the topic.

I am deeply grateful to Dr. Aniruddha Dey for giving me the incredible opportunity to participate in an online research project hosted by one of the leading institutions in nuclear and high-energy physics. His numerous lectures and guidance sessions were invaluable, and without them, completing this project would have been impossible. I am particularly thankful for his support in sharing experimental spectra, relevant literature, and assisting me with computational tasks, from software installation to plotting the final results. Despite his demanding schedule, he consistently provided thoughtful feedback on my weekly reports and analyses, which played a crucial role in the success of this project. His approachable and supportive demeanor made the learning experience even more enriching.

In the later stages of the project, when it was time to write the final report, I took the opportunity to learn LaTeX, having previously worked exclusively with Word. As a beginner, this transition was challenging. Tasks like writing formulas, inserting graphs accurately, adding captions, and filling tables were initially difficult. However, with time, practice, and the help of online tutorials, I gradually became more comfortable with LaTeX. This new skill has been an invaluable addition to my research toolkit.

Abstract

Prompt gamma-ray spectroscopy is a powerful technique for analyzing gamma rays emitted immediately following nuclear reactions, such as neutron capture. It provides valuable insights into elemental and isotopic compositions and is widely used in nuclear physics and materials science.

This report comprehensively explores the basic fundamental ideas behind theoretical, computational, and experimental aspects of gamma-ray spectroscopy measurement technique. Theoretical work includes a detailed derivation of the Klein-Nishina formula, which describes the angular and energy distribution of photons scattered through the Compton effect, followed by simulation code development using C programming to describe the differential cross-section for Compton scattering of photons at different energies. We study the various γ interactions mechanisms like the photoelectric effect, Compton scattering, and pair production. The present work aims to understand the γ detector mechanisms with a focus on the HPGe detectors. The ideality of germanium as a material for gamma detection has been established through a comparative analysis of attenuation coefficients. During the study, a composite type of detector—the Clover detector—is used to study the standard radioactive sources.Clover detectors, known for their high efficiency and resolution, are discussed, with focus on their configuration and capabilities.

The utilization of Clover detectors, which offer superior energy resolution and efficiency, is discussed in detail. The report also provides a comprehensive overview of the RADWARE software package, including its installation and analysis capabilities. To demonstrate the practical application of PGS, the report includes a step-by-step guide on the calibration of a Clover detector using RADWARE. Level schemes of ^{133}Ba and ^{152}Eu isotopes were constructed using the (GLS).The spectrums from the standard sources were then utilized to calibrate the Clover detector. The calibration was performed using linear and quadratic fitting functions.

1.Introduction and motivation

Motivation of the work

Spectroscopy is a scientific technique used to study the interaction between matter and electromagnetic radiation as a function of wavelength, frequency, or energy. It is widely used across various fields of science and engineering to understand the properties of materials, chemical compositions, atomic and molecular structures, and physical processes.Gamma-ray spectroscopy is a critical tool in nuclear physics, astrophysics, material science, and many other fields due to its ability to provide detailed insights into the properties of atomic nuclei and the materials emitting gamma radiation. A deeper understanding of gamma-ray interactions with matter is essential to improve detector technologies and analytical methods. This work aims to bridge theoretical, computational, and experimental aspects of PGS to develop a comprehensive framework for its effective utilization. By deriving fundamental principles like the Klein-Nishina formula, modeling interaction mechanisms, and employing advanced detector systems such as Clover detectors, this study seeks to enhance the precision and reliability of PGS applications. Furthermore, practical aspects like detector calibration and spectrum analysis using tools such as RADWARE, and the construction of nuclear level schemes , underline the importance of integrating cutting-edge technologies and methodologies. Ultimately, this work contributes to the broader goal of advancing nuclear spectroscopy techniques, fostering innovation in research, and enabling new scientific discoveries in nuclear structure and reaction dynamics.

Gamma-ray spectroscopy

Gamma-ray spectroscopy is a technique used to study the properties of gamma (γ) rays emitted by atomic nuclei during transitions between energy levels. These transitions occur when nuclei release energy to move from an excited state to a lower energy state, often producing gamma rays with energies ranging from hundreds of keV to several MeV. The study of these gamma rays provides valuable insights into the structure and behavior of atomic nuclei. Spectroscopy, in general, involves analyzing the "spectrum" of emitted radiation to gain detailed information. In gamma-ray spectroscopy, the focus is on gamma-ray emissions, which reveal critical properties of the emitting nuclei, such as energy levels, intensities, spin states, parities, electromagnetic transitions, and lifetimes. These gamma rays uniquely characterize atomic nuclei and serve as a powerful tool for nuclear structure studies.

Gamma-ray spectroscopy plays a key role in various areas of nuclear science and has several important applications [1]:

1. **Nuclear Structure Studies**
    - Gamma-ray spectroscopy helps in understanding the energy levels of atomic nuclei, which are crucial for mapping the nuclear structure.
    - *Energy levels*: States that the nucleus can occupy.
    - *Spin and parity*: Quantum mechanical properties of these states.
2. **Decay and Reaction Analysis**

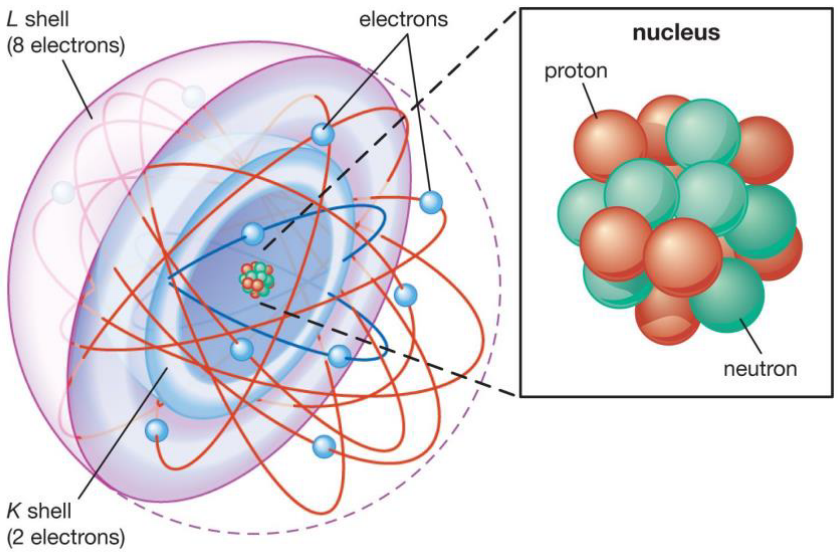

Figure 1: Nuclear structure shells

- Gamma-ray emissions often follow nuclear decay processes such as alpha, beta, or spontaneous fission.
- Spectroscopy enables:
  - Identification of isotopes based on their unique gamma-ray fingerprints.
  - Measurement of half-lives and branching ratios, which are crucial for understanding radioactive decay pathways.
  - Analysis of nuclear reactions, providing data on reaction products and mechanisms.

However, improving gamma-ray spectroscopy in nuclear physics is crucial for advancing our understanding of atomic nuclei, nuclear reactions, and decay processes. It provides clearer, more accurate, and more detailed data that enable scientists to probe nuclear structure, test theoretical models, and explore new phenomena in nuclear science.
These are the primary reasons for advancing gamma-ray spectroscopy in nuclear physics:

1. Improved Sensitivity for Rare Isotopes
2. Higher Energy Resolution
3. Better Background Rejection
4. Broader Detection Range
5. Improved Gamma-Ray Detection Efficiency

In this project, we highlight the need for HPGe detectors in high-resolution gamma spectroscopy. This will be followed by the characterization of individual germanium crystals of a Clover detector. The study aims to provide the detector characterization of a composite Germanium Clover detector.

2.Gamma-ray fundamentals and interaction mechanisms

There are three major types of interactions that play an important role in radiation measurements: photoelectric absorption, Compton scattering, and pair production. All these processes lead to the partial or complete transfer of the gamma-ray photon energy to electron energy. They result in sudden and abrupt changes in the γ-ray photon history, in that the photon either disappears entirely or is scattered through a significant angle.

Gamma radiation

Gamma radiation is short-wave electromagnetic radiation with very high energy In nuclear physics, γ-rays are high-energy photons emitted by atomic nuclei during the processes of nuclear decay or de-excitation. These emissions are a form of electromagnetic radiation, similar to X-rays, but they are typically much more energetic, with photon energies ranging from keV (kilo-electron volts) to MeV (mega-electron volts as shown in Fig.3).

Gamma rays have extremely short wavelengths (less than 10 picometers), corresponding to very high frequencies in the electromagnetic spectrum.

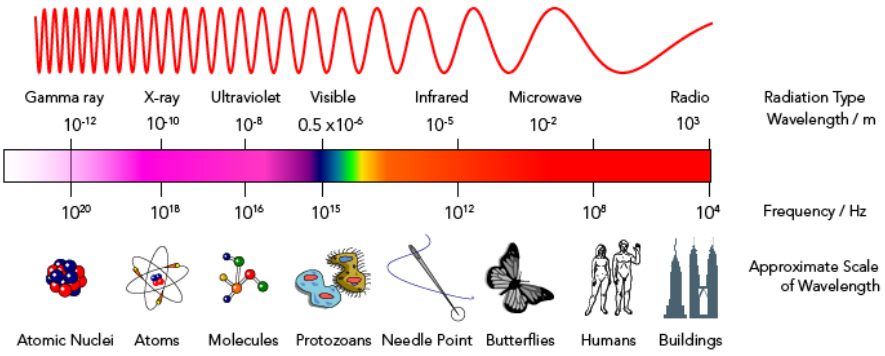

Figure 2: Electromagnetic spectrum

Gamma rays are emitted during processes such as:

1. Radioactive Decay. Radioactive Decay is the random process in which many unstable nuclei decay by emitting alpha or beta particles, leaving the nucleus in an excited state. To shed this excess energy, the nucleus emits gamma rays.

2. Nuclear Reactions. When a nucleus undergoes reactions such as neutron capture or fission, the resulting nucleus often emits gamma rays to stabilize its energy configuration.

3. De-excitation of Nuclei. If a nucleus is left in an excited state (e.g., after a collision or a reaction), it can de-excite by emitting gamma rays.

Attenuation coefficient

The instrumental detection of any particle or radiation often depends upon the production of charged secondary particles which can be collected to produce an electrical signal. Since photons are uncharged, gamma ray detection depends upon other types of interaction which transfer the gamma energy to electrons within the detector material. In the

following the processes that occur if gamma radiation penetrates the detector material are described. These depend on both the energy of the radiation, as well as the mass number of the absorber material. Thereby, the attenuation coefficient is of central importance. It describes the extent to which the radiant flux of a beam is reduced as it passes through a specific material. In general, the attenuation increases with higher mass number, which is the reason why materials with a high mass number are used for the detector parts and its shielding (see Fig.3). The following considerations are essentially taken from[7, 9].

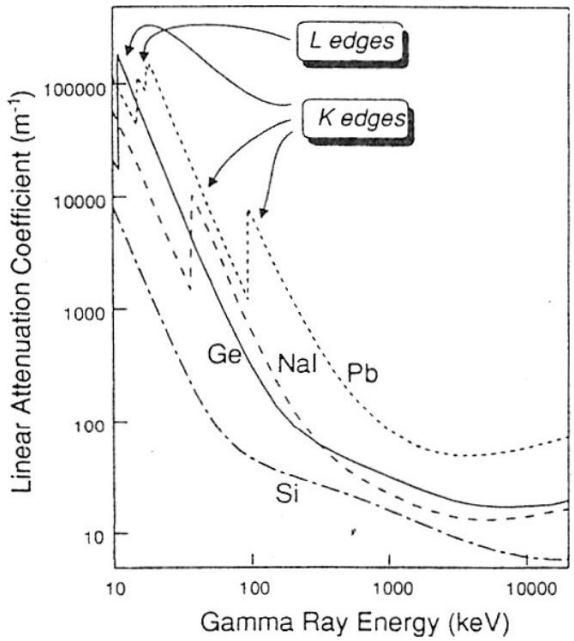

Figure 3: Attenuation coefficient of materials as a function of gamma energy[7]

The linear attenuation coefficient μ is related to the exponential attenuation law, which is given by:

$$I(x) = I_0 e^{-\mu x} \tag{1}$$

where:

- $I(x)$ is the intensity of the radiation after traveling through a material of thickness x.
- I_0 is the initial intensity of the radiation.
- μ is the linear attenuation coefficient (in units of m^{-1}).
- x is the thickness of the material the radiation passes through (in meters).

The attenuation of radiation is exponential, meaning that the intensity decreases by a factor of $e^{-\mu x}$ as it travels through a material.

The total attenuation coefficient μ is the sum of the contributions from these processes:

$$\mu = \mu_{\text{photoelectric}} + \mu_{\text{compton}} + \mu_{\text{pair production}} \tag{2}$$

The linear attenuation coefficient μ describes the fraction of a beam of particles or photons that is absorbed or scattered per unit distance as it travels through a material.

It is a measure of how much a beam of radiation is attenuated due to absorption and scattering processes.The mass attenuation coefficient in the material of Germanium (Z = 32) as a function of photon energy is shown in Fig.5 [9].

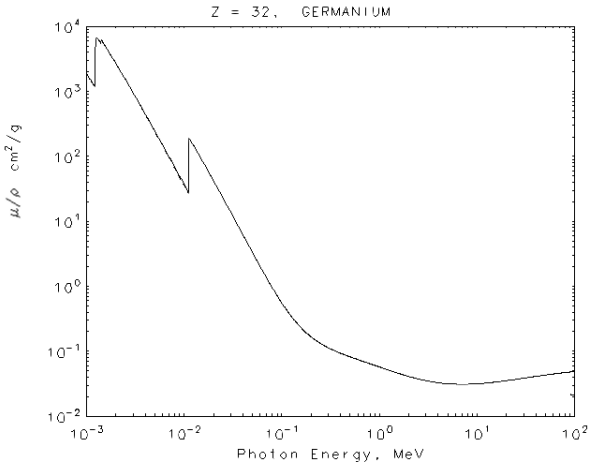

Figure 4: Mass-attenuation coefficient of gamma radiation in germanium as a function of the gamma energy[8]

Photoelectric effect

The electromagnetic radiations, such as γ and X-rays interact with matter in a completely different way. The concepts of range and specific energy loss are not applicable as for charged particles. Electromagnetic radiations have no electric charge and no mass, and their rest mass is zero. They can pass through an absorber without energy loss (i.e., they have a high penetration power). The relationship between energy (E), frequency (ν), and wavelength (λ) is given by:

$$E = h\nu = \frac{hc}{\lambda} \tag{3}$$

where h is Planck's constant

$$h \approx 6.626 \times 10^{-34}\,\text{J·s}$$

In **photoelectric effect** interaction the photon ejects an electron from an atom (generally from the K or L shells). The photon is completely absorbed and all its energy is transferred to the atomic electron. The atom then emits characteristic X–rays and Auger electrons as it returns to normal [2].

Conditions for the Photoelectric Effect

- Photon Energy Greater than Binding Energy The incident photon must have an energy E_{photon} greater than or equal to the binding energy E_{binding} of the electron in its atomic shell.

  $$E_{\text{photon}} \geq E_{\text{binding}}$$

  The binding energy depends on the atomic number (Z) and the electron's orbital. Electrons in inner shells (e.g., K-shell) have higher binding energies.

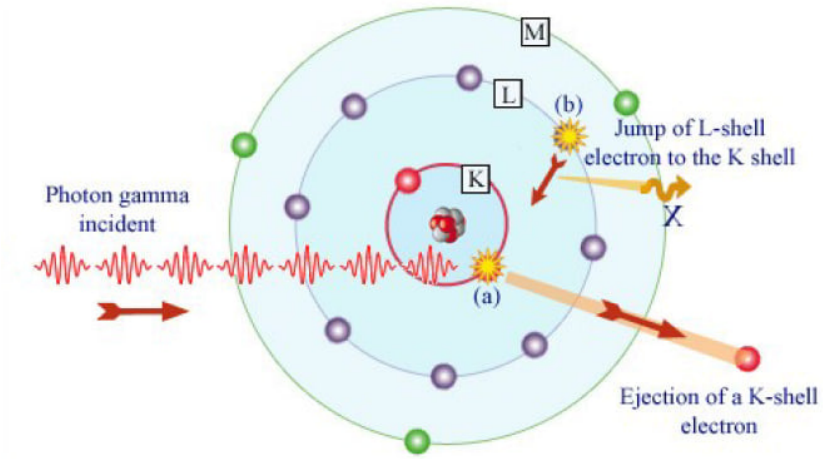

Figure 5: Photoelectric effect.

- Interaction with Bound Electrons

  The photoelectric effect primarily occurs with electrons bound to an atom, as opposed to free electrons. This distinguishes it from other photon-electron interactions like Compton scattering.

  The probability of the photoelectric effect is highest for inner-shell (K or L shell) electrons because they are more tightly bound to the nucleus.

- High Atomic Number (Z) Material

  The cross-section (probability) of the photoelectric effect is proportional to approximately Z^3 or Z^4, depending on the photon's energy.This means elements with higher atomic numbers are more likely to exhibit the photoelectric effect

- Angle of Incidence

  The angle at which the photon interacts with the atom affects the probability of interaction but does not fundamentally change the requirement for the photon's energy[3]

  This mechanism of interaction is very important for γ and x-ray measurements.The photon interacts with the absorber atoms and disappears (i.e., photon absorption occurs). Depending on the photon energy, the most bonded orbital electron in the K or L shell will absorb the photon energy to be removed from the atom with a kinetic energy given by

$$E_{\mathrm{e}} = h\nu - E_{\mathrm{binding}} \tag{4}$$

  where
  E_e = photoelectron kinetic energy,
  $h\nu$ = photon energy,

E_{binding}= electron binding energy.

The photoelectrons are energetic electrons and interact with matter exactly like β particles. These electrons leave the atom and create an electron vacancy in their inner orbit, where either a free electron or an electron from a higher orbit fills this vacancy and generates x-rays. The generated x-rays interact with the absorber and can produce another photoelectron (i.e., photoelectric absorption) with less binding energy (known as an auger electron) than the original photoelectron.

The photoelectric coefficient (τ), the probability of photoelectric absorption per unit length, depends on the photon energy (E) and the absorber atomic number (Z). Photoelectric absorption is the predominant mechanism of interaction for low-energy photons (E_γ). It is enhanced with increasing absorber atomic number (Z). A rough approximation is given by

$$\tau(m^{-1}) \equiv \text{Constant}\frac{Z^n}{E_\gamma^m}. \tag{5}$$

where n and m are constant values that range between 3 and 5[4]

A Free Electron Cannot Absorb All the Energy of a Photon

We will prove that a free electron cannot absorb all the energy of a photon by considering the conservation of momentum and energy.

Initial Conditions

Let the photon have an energy $E_\gamma = h\nu$ and momentum $p_\gamma = \frac{h\nu}{c}$, where h is Planck's constant, ν is the frequency of the photon, and c is the speed of light. This mechanism of interaction is very important for γ and x-ray measurements.The photon interacts with the absorber atoms and disappears (i.e., photon absorption occurs). Depending on the photon energy, the most bonded orbital electron in the K or L shell will absorb the photon energy to be removed from the atom with a kinetic energy given by

The free electron initially has:

- Energy $E_e = m_e c^2$ (rest energy),
- Momentum $p_e = 0$ (electron is at rest).

Conservation of Momentum

When the photon is absorbed by the free electron, the final momentum of the system must equal the initial momentum:

$$p_\gamma + p_e = p_{\text{final}}, \tag{6}$$

where p_{final} is the momentum of the electron after absorbing the photon.

Initially, $p_e = 0$, so:

$$p_\gamma = p_{\text{final}}. \tag{7}$$

The final momentum of the electron is:

$$p_{\text{final}} = \frac{E_{\text{final}}}{c}, \tag{8}$$

where E_{final} is the total energy of the electron after absorption.

Conservation of Energy

The total energy of the system before and after the absorption must also be conserved:

$$E_\gamma + E_e = E_{\text{final}}. \tag{9}$$

Substituting $E_\gamma = h\nu$ and $E_e = m_e c^2$, we get:

$$h\nu + m_e c^2 = E_{\text{final}}. \tag{10}$$

Relativistic Energy-Momentum Relation

The relativistic energy-momentum relation for the electron after absorption is:

$$E_{\text{final}}^2 = (p_{\text{final}} c)^2 + (m_e c^2)^2. \tag{11}$$

Substitute $p_{\text{final}} = \frac{h\nu}{c}$ into the equation:

$$E_{\text{final}}^2 = \left(\frac{h\nu}{c} c\right)^2 + (m_e c^2)^2. \tag{12}$$

Simplify:

$$E_{\text{final}}^2 = (h\nu)^2 + (m_e c^2)^2. \tag{13}$$

Contradiction

From energy conservation:

$$E_{\text{final}} = h\nu + m_e c^2. \tag{14}$$

Square both sides:

$$E_{\text{final}}^2 = (h\nu + m_e c^2)^2. \tag{15}$$

Expand the right-hand side:

$$E_{\text{final}}^2 = (h\nu)^2 + 2h\nu m_e c^2 + (m_e c^2)^2. \tag{16}$$

Comparing with the relativistic energy-momentum relation:

$$E_{\text{final}}^2 = (h\nu)^2 + (m_e c^2)^2. \tag{17}$$

The term $2h\nu m_e c^2$ is missing in the energy-momentum relation, which leads to a contradiction[5].

Summary

This contradiction implies that the assumption of a free electron absorbing all the energy of a photon violates the law of conservation of momentum and energy. Therefore, a free electron cannot absorb all the energy of a photon.

Compton scattering

The interaction process of Compton scattering takes place between the incident gamma-ray photon and an electron in the absorbing material. It is most often the predominant interaction mechanism for gamma-ray energies typical of radioisotope sources.

In Compton scattering, the incoming gamma-ray photon is deflected through an angle 0 with respect to its original direction.The photon transfers a portion of its energy to the electron (assumed to be initially at rest), which is then known as a recoil electron. Because all angles of scattering are possible, the energy transferred to the electron can vary from zero to a large fraction of the gamma-ray energy.

The expression that relates the energy transfer and the scattering angle for any given interaction can simply be derived by writing simultaneous equations for the conservation of energy and momentum. Using the symbols defined in the sketch below

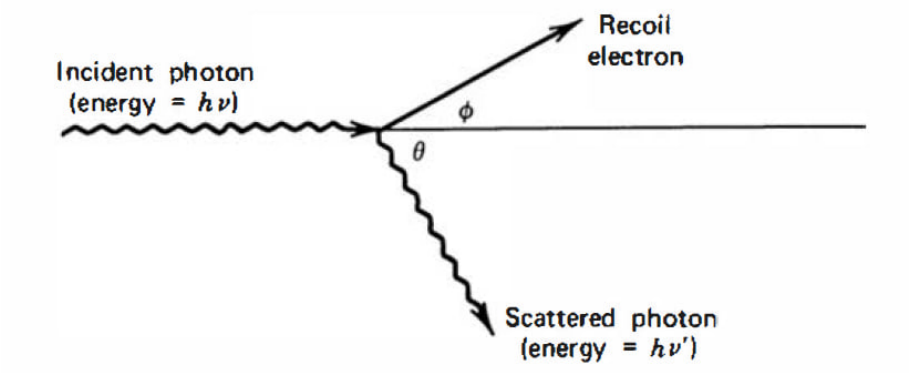

Figure 6: Plot of the scattered photon

we can show that

$$h\nu' = \frac{h\nu}{1 + \frac{h\nu}{m_0 c^2}(1 - \cos\theta)}. \tag{18}$$

where m_0c^2 is the rest-mass energy of the electron (0.511 MeV). For small scattering angles ($\theta \approx 0$), very little energy is transferred. Some of the original energy is always retained by the incident photon, even in the extreme case of $\theta = \pi$ [6].

The probability of Compton scattering per atom of the absorber depends on the number of electrons available as scattering targets and therefore increases linearly with Z.

The angular distribution of scattered gamma rays is predicted by the **Klein-Nishina formula** for the differential scattering cross section $\frac{d\sigma}{d\Omega}$:

$$\frac{d\sigma}{d\Omega} = \frac{r_e^2}{2}\left(\frac{E'}{E}\right)^2\left[\frac{E}{E'} + \frac{E'}{E} - \sin^2\theta\right] \tag{19}$$

where:

- $r_e = \frac{e^2}{4\pi\epsilon_0 m_e c^2}$ is the classical electron radius, which is a fundamental constant in electromagnetic theory.
- E is the energy of the incoming photon,
- E' is the energy of the scattered photon,
- θ is the scattering angle, which is the angle between the incident photon direction and the scattered photon direction.

The formula (20) describes the angular distribution of scattered gamma rays due to Compton scattering. It incorporates both the energy of the incoming and scattered photons, as well as the scattering angle [4]. The formula is valid for a wide range of photon energies and gives the probability of scattering at a specific angle.

Derivation of Klein Nishina formula

Derivation of the High-Energy Limit from the Klein-Nishina Formula

The **Klein-Nishina formula** for the differential cross-section of a photon scattering off a free electron is given by:

$$\frac{d\sigma}{d\Omega} = \frac{r_e^2}{2}\left(\frac{E'}{E}\right)^2\left(\frac{E'}{E} + \frac{E}{E'} - \sin^2\theta\right), \tag{20}$$

From Compton scattering, the energy of the scattered photon is related to the angle θ by:

$$E' = \frac{E}{1 + \frac{E}{mc^2}(1 - \cos\theta)}. \tag{21}$$

For high-energy photons, $E \gg mc^2$, we simplify the expressions for E' and the Klein-Nishina formula under this condition.

From the formula for E':

$$E' = \frac{E}{1 + \frac{E}{mc^2}(1 - \cos\theta)}. \tag{22}$$

In the high-energy limit ($E \gg mc^2$), the term $\frac{E}{mc^2}(1 - \cos\theta)$ dominates. Thus:

$$E' \approx \frac{E}{\frac{E}{mc^2}(1 - \cos\theta)} = \frac{mc^2}{1 - \cos\theta}. \tag{23}$$

This shows that the energy of the scattered photon depends strongly on the scattering angle θ, and at high energies, E' is much smaller than E.

Substitute $E' \approx \frac{mc^2}{1-\cos\theta}$ into the Klein-Nishina formula. The ratio $\frac{E'}{E}$ becomes:

$$\frac{E'}{E} = \frac{\frac{mc^2}{1-\cos\theta}}{E} = \frac{mc^2}{E(1-\cos\theta)}. \tag{24}$$

The Klein-Nishina formula becomes:

$$\frac{d\sigma}{d\Omega} = \frac{r_e^2}{2}\left(\frac{mc^2}{E(1-\cos\theta)}\right)^2\left(\frac{mc^2}{E(1-\cos\theta)} + \frac{E(1-\cos\theta)}{mc^2} - \sin^2\theta\right) \tag{25}$$

The Klein-Nishina formula becomes:

$$\frac{d\sigma}{d\Omega} = \frac{r_e^2}{2}\left(\frac{mc^2}{E(1-\cos\theta)}\right)^2\left(\frac{mc^2}{E(1-\cos\theta)} + \frac{E(1-\cos\theta)}{mc^2} - (1-\cos^2\theta)\right) \tag{26}$$

In the high-energy limit ($E \gg mc^2$):

- The term $\frac{mc^2}{E(1-\cos\theta)}$ dominates.
- The second term $\frac{E(1-\cos\theta)}{mc^2}$ becomes negligible.

Thus, the leading term in the parentheses is:

$$\frac{mc^2}{E(1-\cos\theta)} \tag{27}$$

The differential cross-section becomes approximately:

$$\frac{d\sigma}{d\Omega} \approx \frac{r_e^2}{2}\left(\frac{mc^2}{E(1-\cos\theta)}\right)^4 \tag{28}$$

At very high energies, the scattering is primarily in the forward direction ($\theta \approx 0$), meaning $1-\cos\theta \to 0$. The cross-section depends strongly on the scattering angle θ, with a sharp decrease for larger angles.

In the high-energy limit, the differential cross-section simplifies to:

$$\frac{d\sigma}{d\Omega} \propto \frac{1}{(1-\cos\theta)^4} \tag{29}$$

Derivation of the Thomson Cross-Section from the Klein-Nishina Formula

The **Klein-Nishina formula** for the differential cross-section of a photon scattering off a free electron is given by:

$$\frac{d\sigma}{d\Omega} = \frac{r_e^2}{2}\left(\frac{E'}{E}\right)^2\left(\frac{E'}{E} + \frac{E}{E'} - \sin^2\theta\right) \tag{30}$$

From Compton scattering, the energy of the scattered photon is related to the scattering angle θ by:

$$E' = \frac{E}{1 + \frac{E}{mc^2}(1 - \cos\theta)} \tag{31}$$

In the low-energy limit, $E \ll mc^2$, the term $\frac{E}{mc^2}(1 - \cos\theta)$ becomes negligible. Thus:

$$E' \approx E$$

This implies that:

$$\frac{E'}{E} \approx 1$$

Substituting this approximation into the Klein-Nishina formula simplifies it significantly.

Substitute $\frac{E'}{E} \approx 1$ into the Klein-Nishina formula:

$$\frac{d\sigma}{d\Omega} = \frac{r_e^2}{2}\left(1^2 \cdot \left(1 + 1 - \sin^2\theta\right)\right) \tag{32}$$

Thus, the differential cross-section becomes:

$$\frac{d\sigma}{d\Omega} = \frac{r_e^2}{2}(1 + \cos^2\theta) \tag{33}$$

This is the **Thomson differential cross-section**

The total cross-section is obtained by integrating the differential cross-section over all solid angles:

$$\sigma_T = \int \frac{d\sigma}{d\Omega}\, d\Omega \tag{34}$$

The element of solid angle is $d\Omega = 2\pi\, d\cos\theta$, and $\cos\theta$ ranges from -1 to 1 Substituting $\frac{d\sigma}{d\Omega} = \frac{r_e^2}{2}(1 + \cos^2\theta)$, we have:

$$\sigma_T = \int_0^{2\pi} d\phi \int_{-1}^{1} \frac{r_e^2}{2}(1 + \cos^2\theta)\, d\cos\theta \tag{35}$$

The azimuthal integral over ϕ contributes a factor of 2π:

$$\sigma_T = 2\pi \int_{-1}^{1} \frac{r_e^2}{2}(1 + \cos^2\theta)\, d\cos\theta \tag{36}$$

$$\sigma_T = \pi r_e^2 \int_{-1}^{1} (1 + \cos^2\theta)\, d\cos\theta \tag{37}$$

Now substitute the results into the total cross-section:

$$\sigma_T = \pi r_e^2 \left(\int_{-1}^{1} 1\, d\cos\theta + \int_{-1}^{1} \cos^2\theta\, d\cos\theta \right). \tag{38}$$

$$\sigma_T = \pi r_e^2\,(2 + 1) = \pi r_e^2 \cdot 3.$$

Finally:

$$\sigma_T = \frac{8\pi}{3} r_e^2. \tag{39}$$

This result represents the total cross-section for the scattering of low-energy photons (Thomson scattering).

Code development and simulation os scattering distribution

The Klein-Nishina formula describes the differential cross-section for Compton scattering of photons on free electrons. Below is the C code that computes the differential cross-section for different photon energies and scattering angles, and saves the results to a file for generating a linear and polar plot.

```
#include <stdio.h>
#include <math.h>

// Constants
#define PI 3.141592653589793
#define ELECTRON_REST_MASS 511.0 // Electron rest mass in keV

// Klein-Nishina differential cross-section formula
double klein_nishina(double energy, double theta) {
    double energy_ratio = energy / ELECTRON_REST_MASS;
    double cos_theta = cos(theta);
    double denom = 1.0 + energy_ratio * (1.0 - cos_theta);
    double term1 = pow(1.0 / denom, 2);
    double term2 = 1.0 + pow(cos_theta, 2);
    double term3 = pow(energy_ratio / denom, 2) * (1.0 - cos_theta);
    return 0.5 * term1 * (term2 + term3);
}

int main() {
    double energies[] = {5.0, 50.0, 200.0, 1000.0}; // Photon energies in keV
    int num_energies = sizeof(energies) / sizeof(energies[0]);
    int num_angles = 360; // Number of angles for polar plot
    double theta_step = 2.0 * PI / num_angles; // Step size in radians

    // Open output file for polar plot data
    FILE *output_file = fopen("klein_nishina_polar.dat", "w");
    if (!output_file) {
        perror("Error opening output file");
        return 1;
    }

    // Generate data for each energy
    for (int e = 0; e < num_energies; e++) {
        double energy = energies[e];
        fprintf(output_file, "# Energy = %.2f keV\n", energy);

        for (int i = 0; i < num_angles; i++) {
            double theta = i * theta_step; // Angle in radians
            double d_sigma = klein_nishina(energy, theta);
            fprintf(output_file, "%.6f %.8e\n", theta, d_sigma); // Angle in radians a
        }
        fprintf(output_file, "\n\n");
```

```
    }

    fclose(output_file);

    printf("Data generated and saved to 'klein_nishina_polar.dat'.\n");
    return 0;
}
```

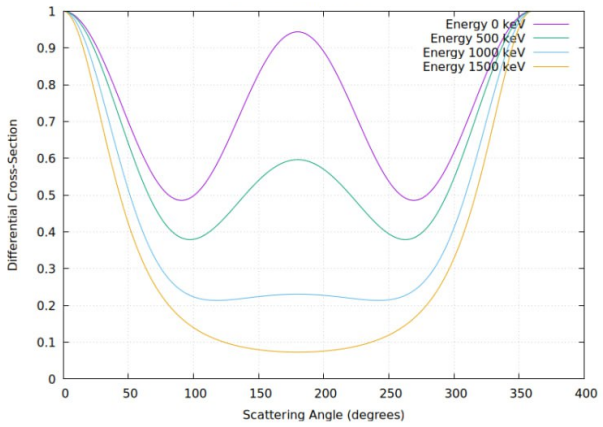

Figure 7: A linear plot of the number of photons scattering angle dependence of differential cross-section at different Energies

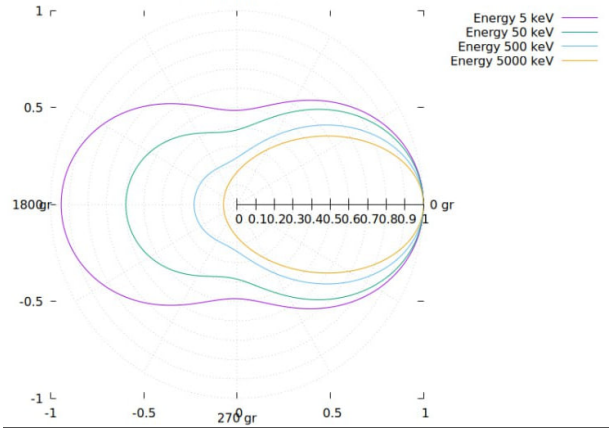

Figure 8: Polar plot distribution of differential cross-section for photon-nucleus sScattering at different energies

Pair production

In pair production, a photon of sufficiently high energy is annihilated and an electron–positron pair is created. For a free photon, conservation of energy and momentum would not be possible, so pair production must take place in the field of a nucleus (or of another electron) which will take up the balance of momentum. The energy threshold for this process is $2mc^2$ or 1.02 MeV.

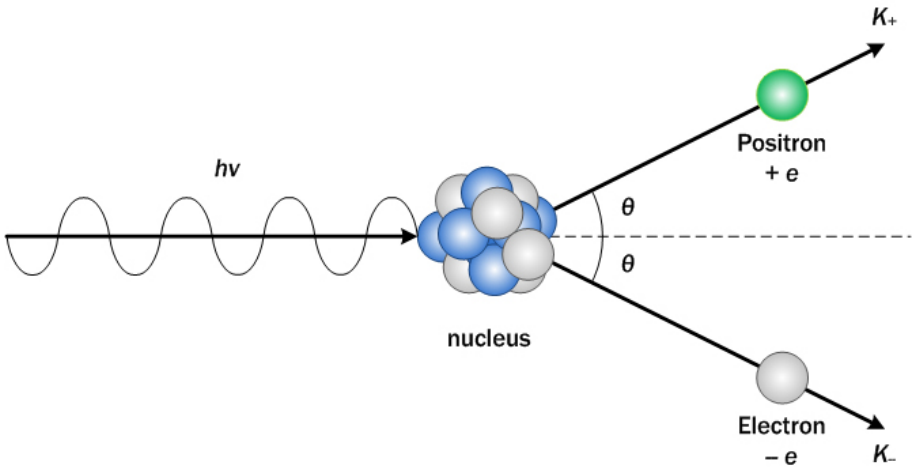

Figure 9: Pair Production

If the gamma-ray energy exceeds twice the rest-mass energy of an electron (1.02 MeV), the process of pair production is energetically possible. As a practical matter, the probability of this interaction remains very low until the gamma-ray energy approaches several MeV, and therefore pair production is predominantly confined to high-energy gamma rays. In the interaction (which must take place in the Coulomb field of a nucleus), the gamma-ray photon disappears and is replaced by an electron-positron pair. All the excess energy carried in by the photon above the 1.02 MeV required to create the pair goes into kinetic energy shared by the positron and the electron. Because the positron will subsequently annihilate after slowing down in the absorbing medium, two annihilation photons are normally produced as secondary products of the interaction.

The cross-section for pair production in the nuclear field depends on the photon energy and the atomic number Z of the nucleus. It is given by the relation [6]:

$$\sigma_{\text{pair production}} \propto Z^2, \tag{40}$$

where:

- $\sigma_{\text{pair production}}$ is the pair production cross-section,
- Z is the atomic number of the nucleus.

The exact value of the cross-section is obtained from quantum electrodynamics (QED) calculations and increases with the photon energy. At high photon energies, the cross-section grows approximately logarithmically with energy due to the dependence of the pair production process on the Coulomb field of the nucleus.

3.Semiconductor detectors and HPGe Clover

Why Semiconductors?

A **semiconductor** is a material that has electrical conductivity between that of a conductor (like metals) and an insulator (like rubber). This means that semiconductors can conduct electricity, but not as well as metals. The key feature of semiconductors is that their conductivity can be controlled by adding impurities (a process called *doping*) or by changing conditions like temperature or light exposure.

Semiconductors are materials that do not have enough free charge carriers to behave as electrical conductors or a high resistivity to act as electrical insulators. The solid crystal has three energy bands: the valence band, the conduction band, and the forbidden band.

For electrical conductors, the width of the forbidden energy band is very small. This allows the movement of valence electrons to the conduction band under the effect of any electric field strength higher than zero, where the electrons can move freely in the crystal lattice and carry electric current.

For electrical insulators, the width of the forbidden energy band is large (about 10 eV), enough to prevent the movement of valence electrons to the conduction band, which is completely empty.

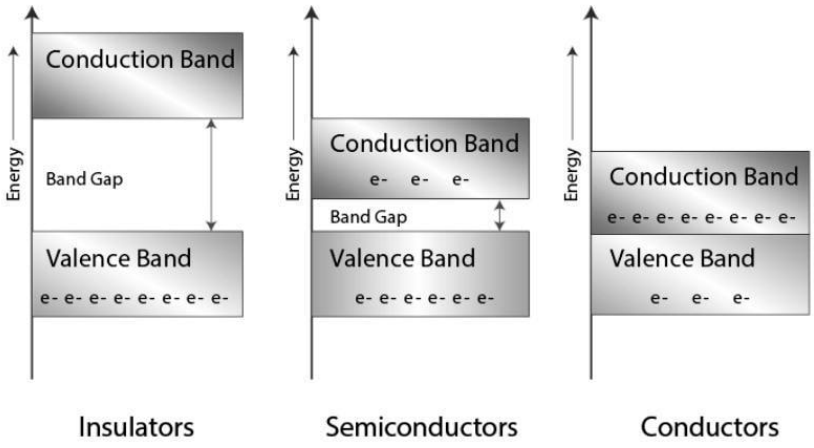

Figure 10: The band structure of different types of materials

For semiconductor materials, the forbidden energy band is relatively narrow, to prevent the movement of electrons to the conduction band at low temperatures (i.e., the conductivity of the semiconductors is zero). As temperature increases, some electrons gain enough energy to cross the forbidden band to the conduction band, where electrons can carry electric current under the influence of an electric field in the same way as conductors. Semiconductor crystals as a detector material should have the capability of supporting large electric field gradients, high resistivity, and exhibit long life and mobility for both electrons and holes. If the mobility is too small and lifetime is too short, most electrons and holes will be trapped in crystal lattice imperfections or recombine before they can be collected.

The group IV elements silicon and germanium are the most widely used semiconductor

crystals as radiation detectors. Some of the key characteristics of various semiconductors for radiation detectors are shown below in the table 1.

The conductivity of semiconductors increases with an increase in the concentration of impurities, which create new energy levels that facilitate the movement of the carrier within the crystal. The ideal semiconductor material is "intrinsic" or "low effective impurity" material that is produced by a process called "doping," which involves the addition of an impurity to reduce the charge carrier concentration (i.e., adding an electron-accepting impurity to compensate for electron donor impurities) [4].

Although doping increases the resistivity of the material, it also increases the probability of electron-hole trapping or recombination.

Material	Z	Band gap (eV)	Energy/E_h pair (eV)
Si	14	1.12	3.61
Ge	32	0.74	2.98
CdTe	48-52	1.47	4.43
HgI_2	80-53	2.13	6.5
GaAs	31-33	1.43	5.2

Table 1: Table of materials with their band gaps and energy per electron-hole pair.

Choice of Silicon (Si) and Germanium (Ge) for Different Applications

The choice of **silicon (Si)** for charged particle spectroscopy and **germanium (Ge)** for gamma-ray detection is based on the specific physical and electronic properties of these materials, which make them best suited for their respective applications.

- Silicon (Si): Best for charged particle spectroscopy because of its optimal band gap, ability to measure energy deposition with high resolution, low atomic number (minimizing gamma-ray interactions), and excellent fabrication properties.
- Germanium (Ge): Preferred for gamma-ray detection due to its high atomic number (enhancing gamma-ray interaction), smaller band gap (higher efficiency), and superior energy resolution critical for gamma-ray spectroscopy.

Semiconductor detectors are thermally sensitive due to their narrow energy band gap (0.74 eV for germanium and 1.12 eV for silicon). To reduce thermal noise, both germanium and silicon photon detectors are cooled with liquid nitrogen during operation. This lowers the reverse leakage current to the range of 10^{-10} to 10^{-12} A at liquid nitrogen temperature (77 K).

Semiconductor detectors offer superior energy resolution compared to gas-filled and scintillation detectors. This is due to the larger number of charge carriers produced per incident radiation, leading to improved statistics and better energy resolution.

Germanium is widely used for γ and X-ray detection, while silicon is used for X-rays (as Si(Li) detectors) and charged particles (as silicon surface barrier detectors). NaI(Tl) scintillators have a higher detection efficiency than semiconductor detectors due to their high atomic number.

However, semiconductor detectors have advantages over NaI(Tl) scintillators, including:

- High energy resolution
- Compact size
- Relatively fast timing characteristics

Their disadvantages include:

- Limited size
- Requirement for cooling in some cases
- Sensitivity to radiation-induced damage

Gamma-ray detectors

Germanium, with its high atomic number ($Z = 32$), offers greater gamma-ray interaction probability compared to silicon, as discussed in Chapter 2. To improve electrical conductivity, extrinsic semiconductors are employed.

The depletion region's width (d) at the p-n junction can be determined using the Poisson equation:

$$d = \sqrt{\frac{2\epsilon V}{N}}$$

Here, V represents the applied bias voltage, ϵ is the vacuum permittivity, and N is the concentration of impurities in the material.

The depletion width (d) increases significantly as the impurity concentration (N) decreases, as evident from the above equation. This characteristic explains why highly pure germanium, with impurity levels as low as 10^{10} atoms/cm^3, is ideal for use in gamma-ray spectroscopy.

HPGe clover detector

The **Clover High-Purity Germanium (HPGe) detector** is an advanced radiation detection instrument. It comprises four HPGe crystals arranged in a close-packed cloverleaf configuration within a single cryostat. While each crystal operates independently, they are housed together, providing both high detection efficiency and versatility. The detector achieves a high absolute efficiency due to its large active volume and its ability to recover scattered gamma rays through the *add-back mechanism* [10].

The clover detector, consists of four closely-packed n-type hyperpure germanium crystals.In the CLOVER detector assembly, the crystals are held on a minimized crystal holder to reduce the quantity of material surrounding the crystals and to improve the peak-to-background ratio.The geometry of the crystals inside the vacuum chamber is shown in Fig. 12. Each of these crystals, with a 50 mm diameter and 70 mm length, has a tapering at the front faces, leaving a total volume of 470 cm^3, which is nearly 89% of the initial volume. Moreover, the crystals are packed very closely together to improve the add-back

factor. The maximum gap between two adjacent crystals is ≤ 0.7 mm without any absorbent material along the whole crystal length that will absorb more than 1% of 20 keV gamma rays.

A common high-voltage supply provides a positive bias of +2500 V (max) to the inner side of the crystal with p-type contact in all four crystals. The detector was placed on a horizontal stand custom-made to support the detector and the liquid N_2 dewar. The HPGe crystals were maintained at liquid N_2 temperature by pressure-filling the dewar every 24 hours.

The LED display glows and automatically cuts off the bias from the detector in the event of detector warm-up.

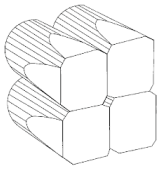

Figure 11: Inside the vacuum chamber

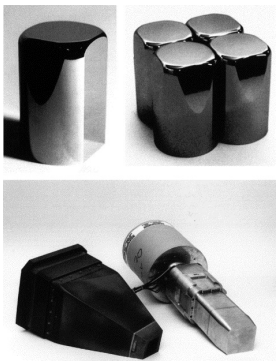

Figure 12: Germanium crystal arrangement inside a clover

A major advantage of a CLOVER detector consists of its high absorption efficiency: results are not only four times those obtained with a single crystal but, as crystals are mounted without any additional absorbing material, the full energy of a photon Compton scattered and absorbed in a second (or even a third) crystal can be determined. The full energy peak can be obtained by summing ("add-back") the energies deposited in the N segments firing .The "Add-back" efficiency is then superior to the sum of the four individual efficiencies[11].

CLOVER detector Dewars are small and allow:

- Compact arrangement covering nearly 4π.
- Positioning in all directions without significant temperature change.
- Full 1-day LN_2 holding time.

4.RADWARE:An interactive graphical analysis software

Installation

I have successfully accessed the Radware software installation files from the official website: https://radware.phy.ornl.gov/.After that I installed required dependencies, which is given in README folder [12].

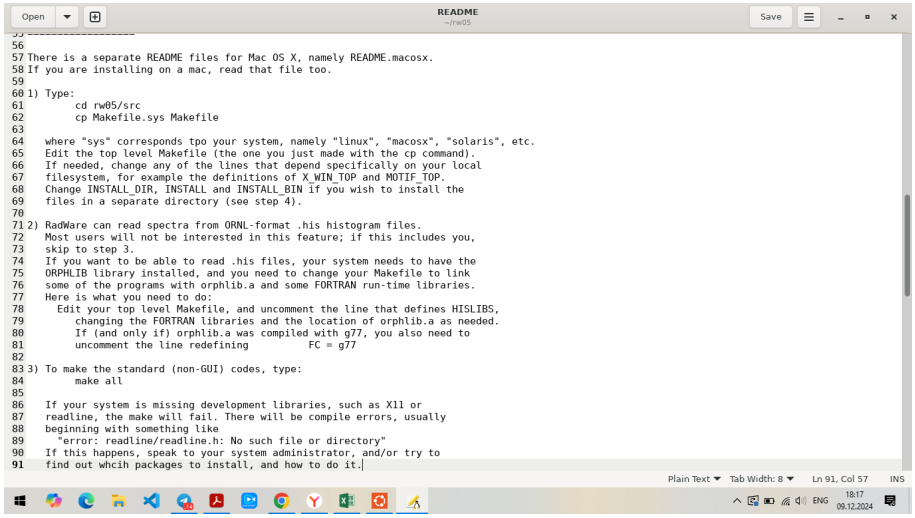

Figure 13: Steps of installing Radware software packages

Different packages and commands

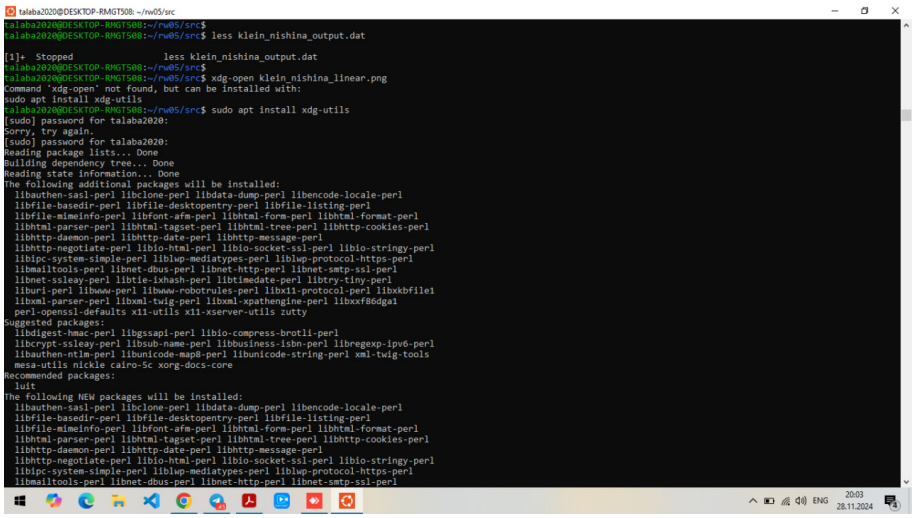

Figure 14: Updating packages through gnuplot

Main commands for Radware software:

- sudo apt update- update packages
- dir - show folder

- mkdir - create folder
- touch filename.c - create file
- gedit filename.c - open file
- gcc -o filename filename.c - open output file
- nano filename.png - open to edit
- eog filename.png - show in macroc in .png format

GLS and GF3 commands :

- x -out og command
- st - exit command
- sp -reading command
- ds1 -display command
- ls -ahlrt - to see created files
- ex - expand command
- cr - shift with cursor command
- pf -peak find command
- ec -energy calibration

Utilization of ENSDF database

The Evaluated Nuclear Structure Data File (ENSDF) provides comprehensive nuclear structure and decay data for various isotopes. To utilize this database for specific isotopic data, the following steps are followed:

1. **Accessing the ENSDF Database**: Open the Nuclear Data Center (NNDC) website, which hosts the ENSDF database.
2. **Selecting ENSDF**: From the NNDC homepage, navigate to the ENSDF section, which contains evaluated nuclear structure data. This section provides detailed information about isotopic energy levels, gamma transitions, half-lives, and other nuclear properties.
3. **Searching for an Isotope**: In the ENSDF interface, enter the name or mass number of the desired isotope into the search bar. The system retrieves the evaluated nuclear data for the isotope, including its level schemes, gamma-ray transitions, and decay characteristics.

This process enables researchers to gather precise and reliable nuclear data, which is essential for analyzing gamma-ray spectroscopy results, preparing level schemes, and interpreting nuclear reactions or decays.

The ENSDF database is an invaluable tool for experimental nuclear physics, providing critical data for simulations, calibrations, and comparison with experimental results.

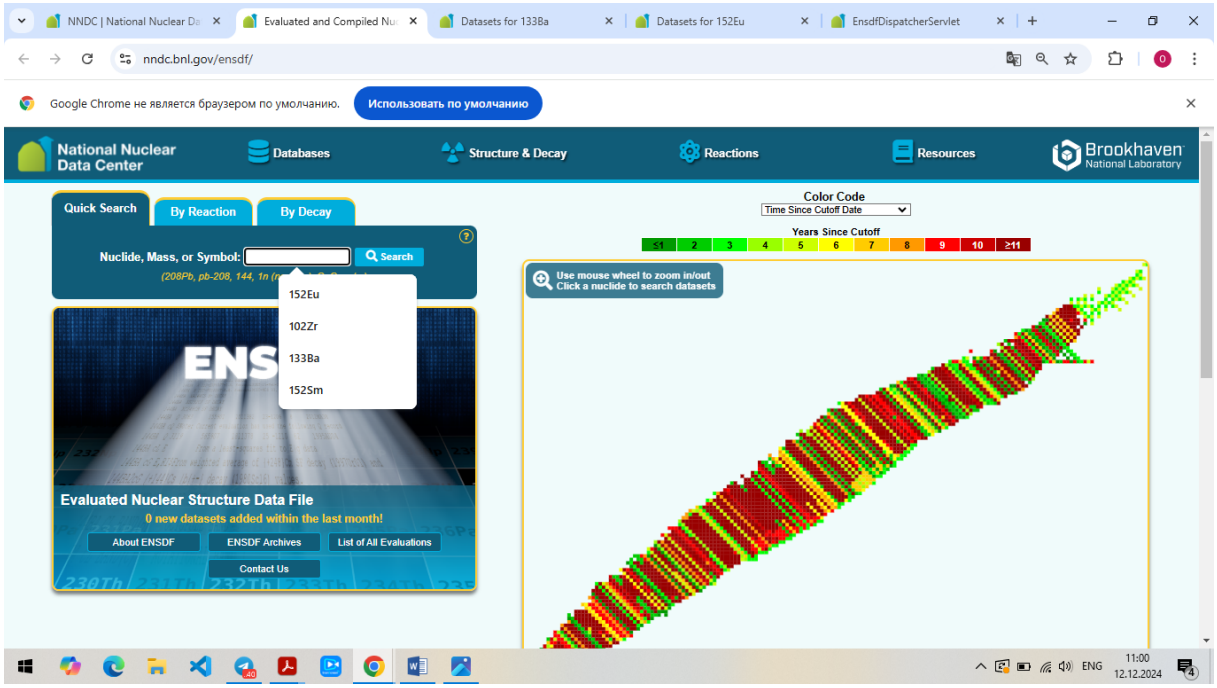

Figure 15: Accessing the ENSDF Database

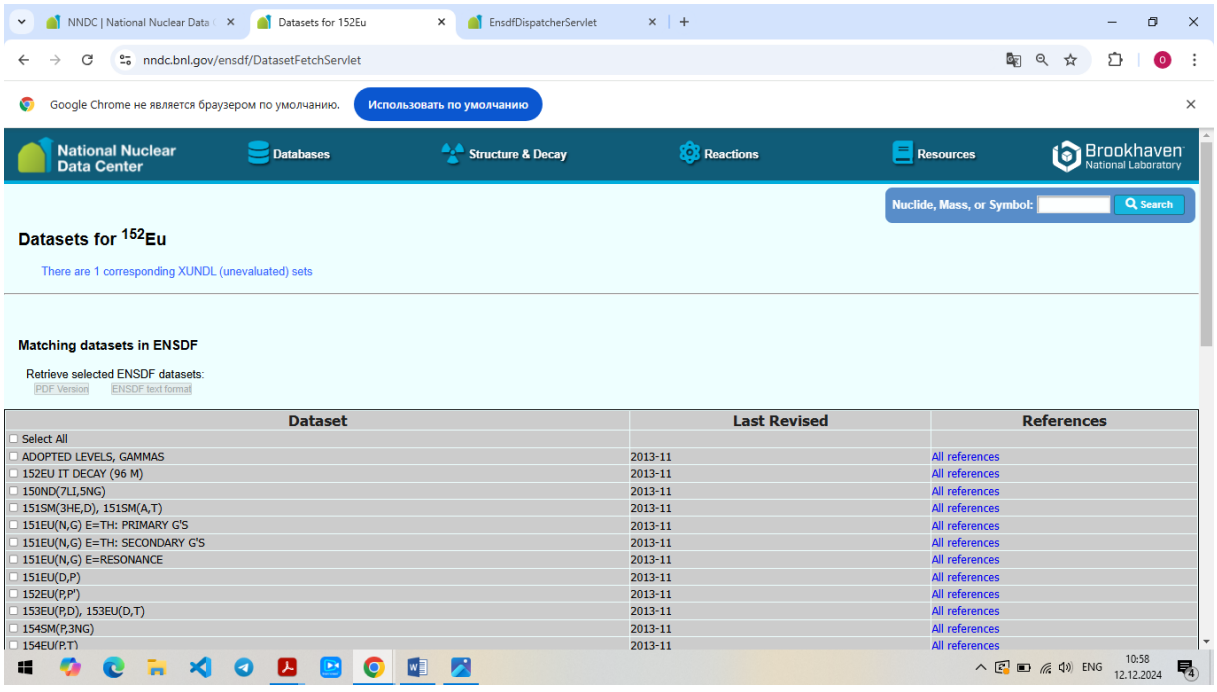

Figure 16: Searching for an isotope

Nuclei level scheme development

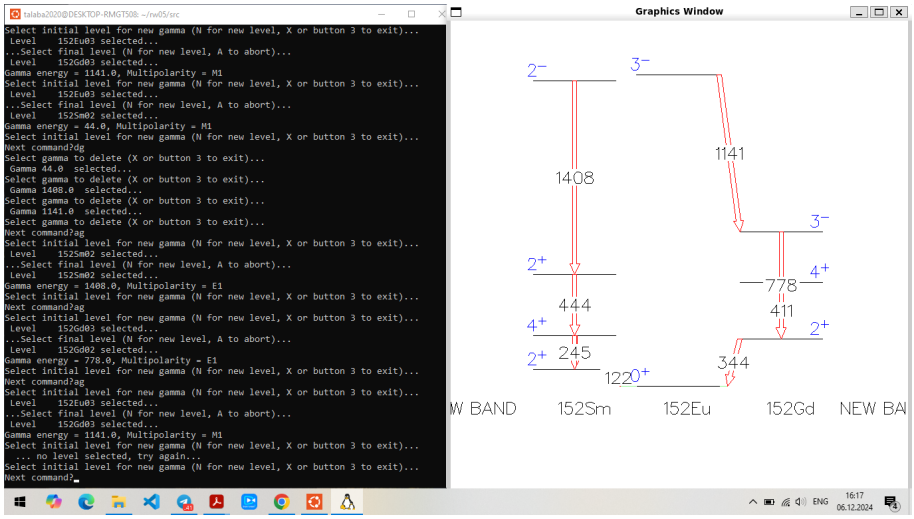

Figure 17: GLS code for plotting ^{152}Eu isotope

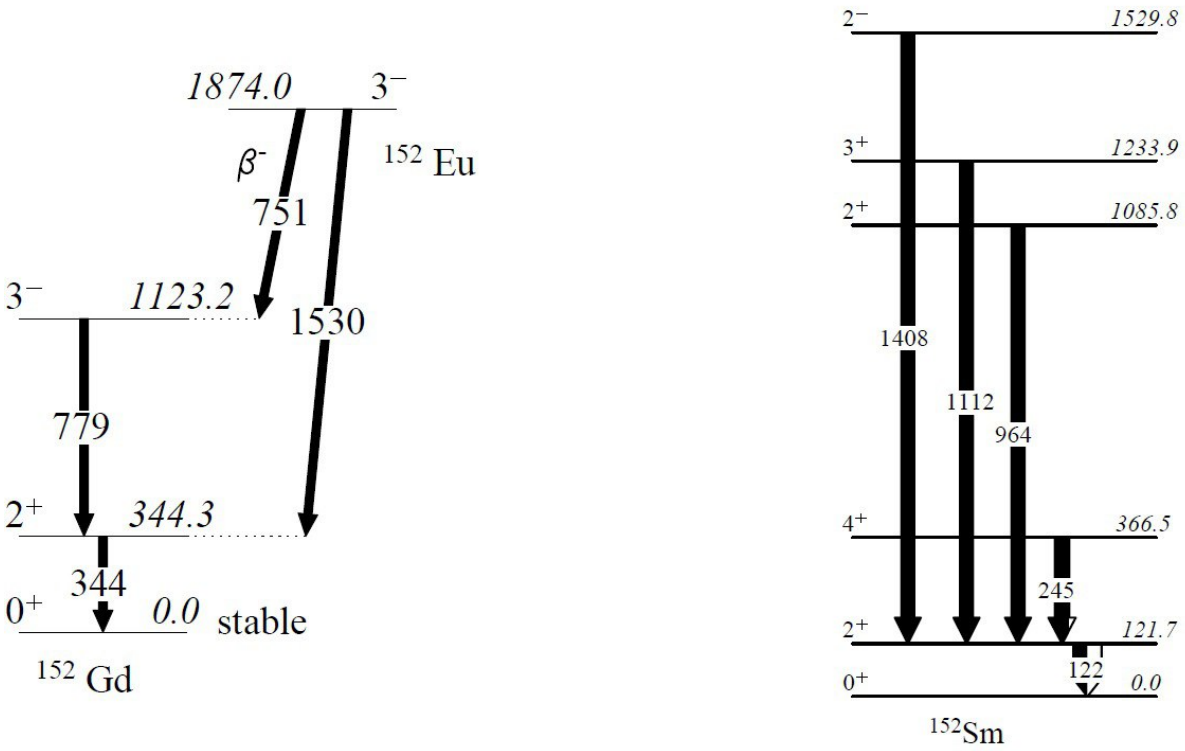

Figure 18: Eight of the gamma energy from the decay of ^{152}Eu isotope were used to calibrate

5.Data processing and analysis using RADWARE software

Spectrums of uncalibrated detector crystals

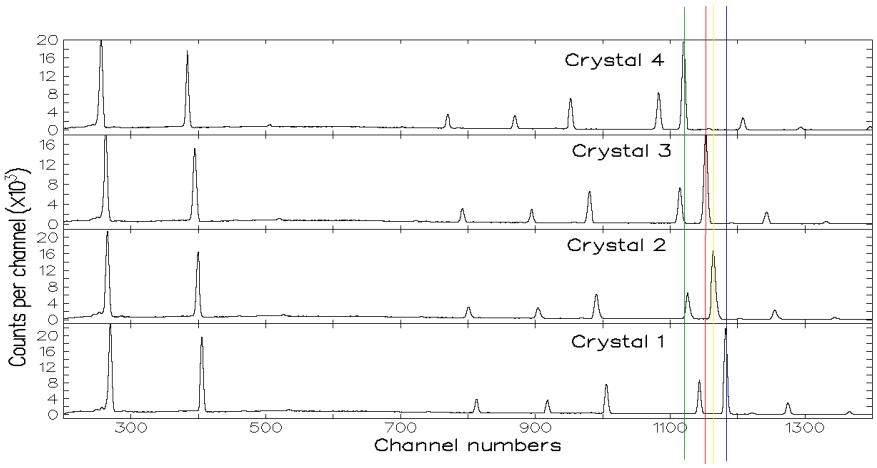

Figure 19: Uncalibrated spectra of peaks obtained from the ^{152}Eu and ^{133}Ba sources

Why the shift increases with energy?

- At low energies, the effects of nonlinearity, charge collection issues, and gain drift are minimal because the signals are smaller, and the response is closer to linear.
- At higher energies:
  - The signal amplitude increases, magnifying nonlinearity in the electronics.
  - Charge collection inefficiencies or recombination effects become more noticeable.
  - Errors in calibration (e.g., higher-order terms in the calibration function) have a larger impact.

Peak fitting and Calibration using RADWARE

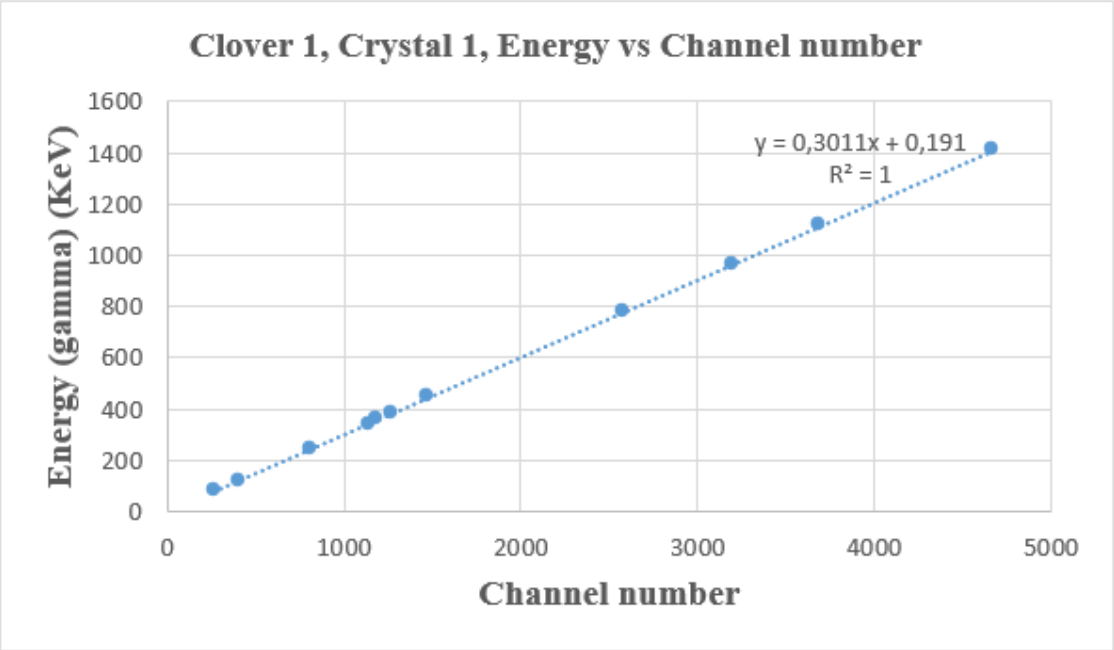

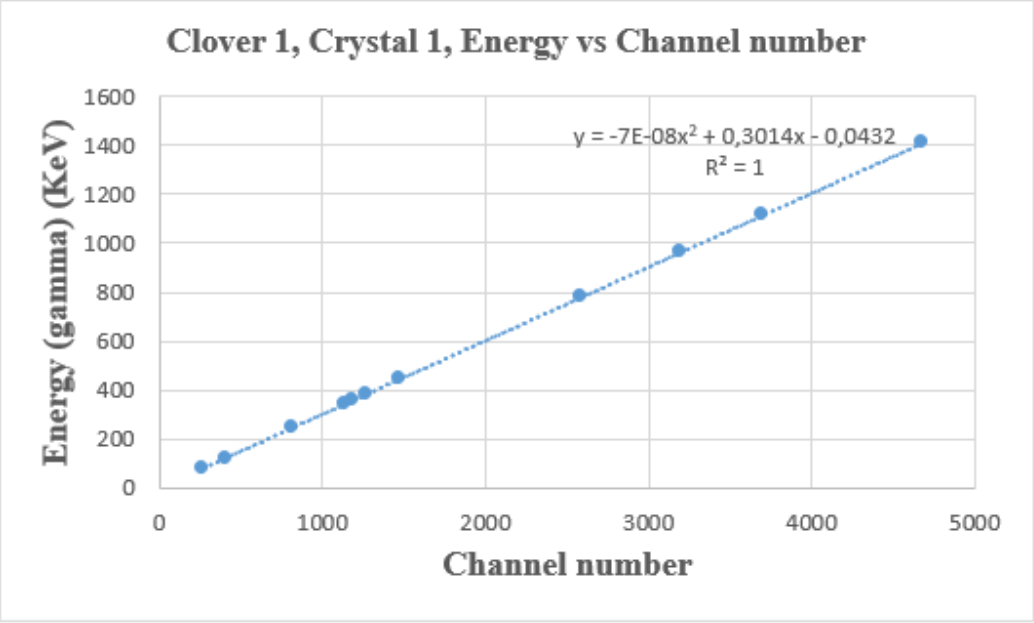

Figure 20: Energy calibration of Clover 1, Crystal 1 using a linear and quadratic fit function

Source	Channel number	Energy (gamma) (keV)	Calculated (linear)	Calculated (quadratic)	Residual (linear)	Residual (quadratic)
^{133}Ba	268	80,999	**80,8858**	**80,7269732**	-0,1132	-0,27202768
^{152}Eu	405	121,783	**122,1365**	**122,0213183**	0,3535	0,22931825
^{152}Eu	812	244,692	**244,6842**	**244,6474459**	-0,0078	-0,04455408
^{152}Eu	1143	344,276	**344,3483**	**344,3655486**	0,0723	0,08954857
^{133}Ba	1182	356,01	**356,0912**	**356,1138013**	0,0812	0,10380132
^{133}Ba	1274	383,86	**383,7924**	**383,8267847**	-0,0676	-0,03321532
^{152}Eu	1474	443,976	**444,0124**	**444,0683127**	0,0364	0,09231268
^{152}Eu	2586	778,903	**778,8356**	**778,9090823**	-0,0674	0,00608238
^{152}Eu	3201	964,131	**964,0112**	**964,0209519**	-0,1189	-0,11004807
^{152}Eu	3693	1112,116	**1112,1533**	**1112,072323**	0,0373	-0,04367743
^{152}Eu	4677	1408,011	**1408,4357**	**1408,073397**	0,4247	0,06239697

Table 2: Gamma energy data with linear and quadratic calculations and residuals for Clover 1, Crystal 1

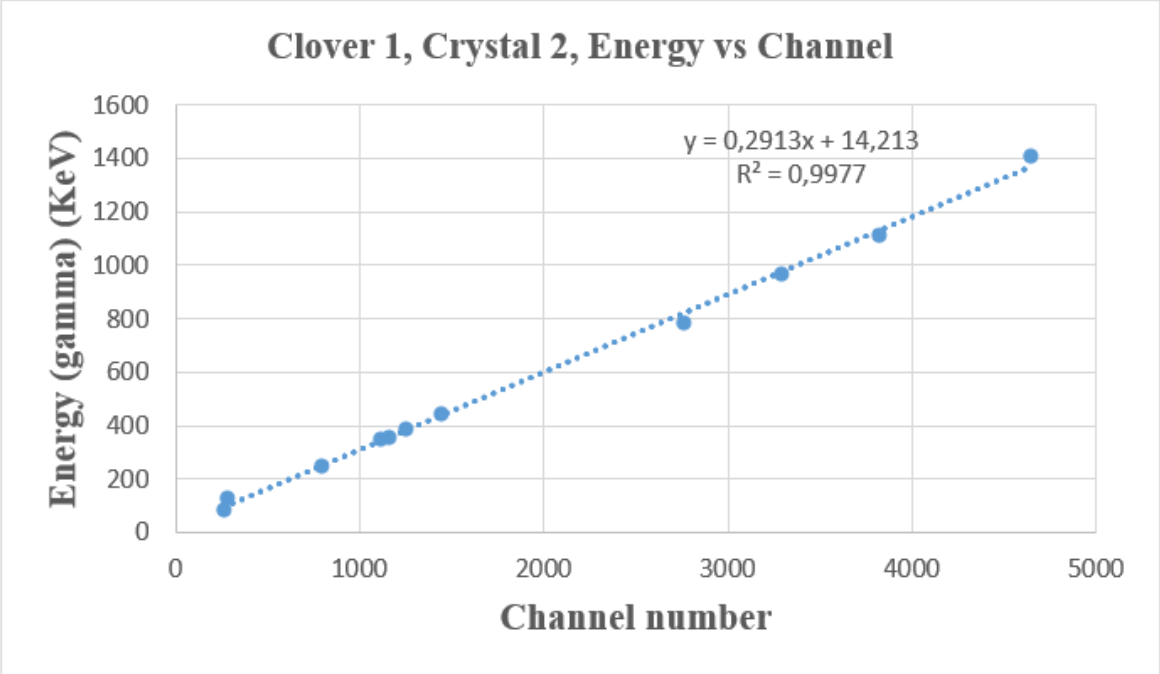

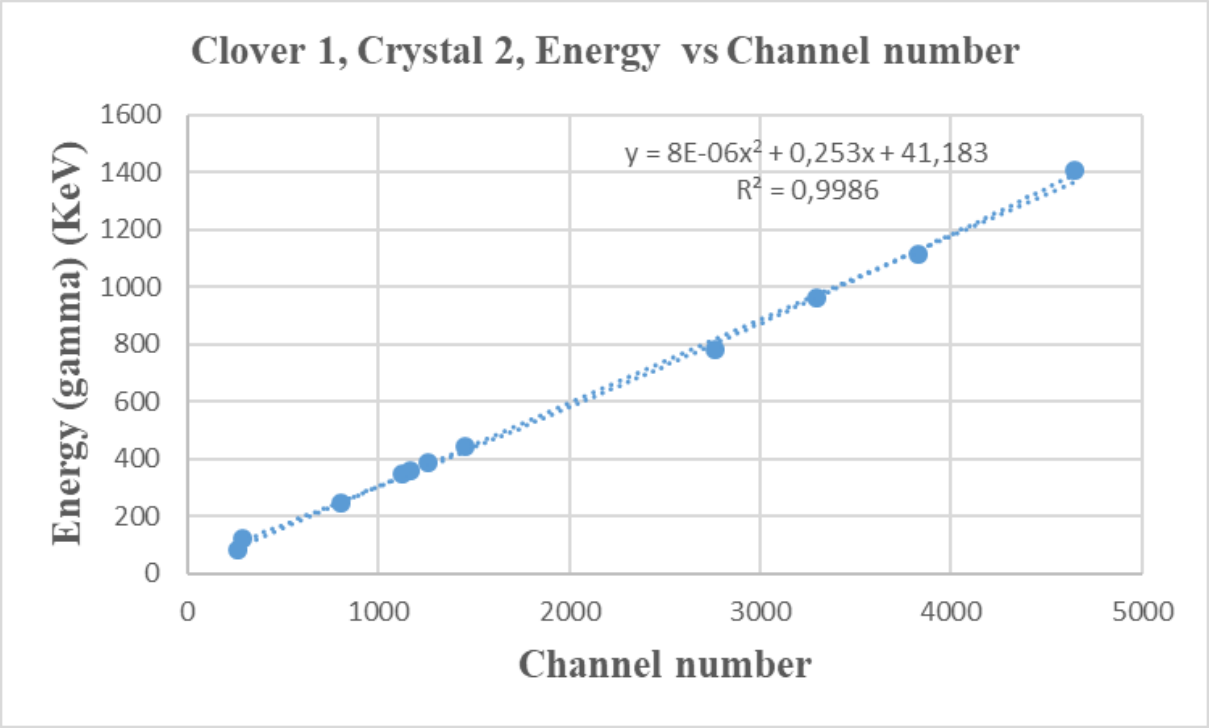

Figure 21: Energy calibration of Clover 1, Crystal 2 using a linear and quadratic fit function

Source	Channel Number	Energy (Gamma) (keV)	Calculated (Linear)	Calculated (Quadratic)	Residual (Linear)	Residual (Quadratic)
^{133}Ba	264	80.999	**91.1162**	**108.5326**	10.1172	27.5336
^{152}Eu	285	121.783	**97.2335**	**113.9378**	-24.5495	-7.8452
^{152}Eu	800	244.692	**247.2530**	**248.7030**	2.5610	4.0110
^{152}Eu	1125	344.276	**341.9255**	**335.9330**	-2.3505	-8.3430
^{133}Ba	1164	356.010	**353.2862**	**346.5142**	-2.7238	-9.4958
^{133}Ba	1257	383.860	**380.3771**	**371.8444**	-3.4829	-12.0151
^{152}Eu	1454	443.976	**437.7632**	**425.9579**	-6.2128	-18.0181
^{152}Eu	2761	778.903	**818.4923**	**800.7010**	39.5893	21.7980
^{152}Eu	3293	964.131	**973.4639**	**961.0628**	9.3329	-3.0682
^{152}Eu	3832	1112.116	**1130.4746**	**1128.1528**	18.3586	16.0368

Table 3: Gamma energy data with linear and quadratic calculations and residuals for Clover 1, Crystal 2

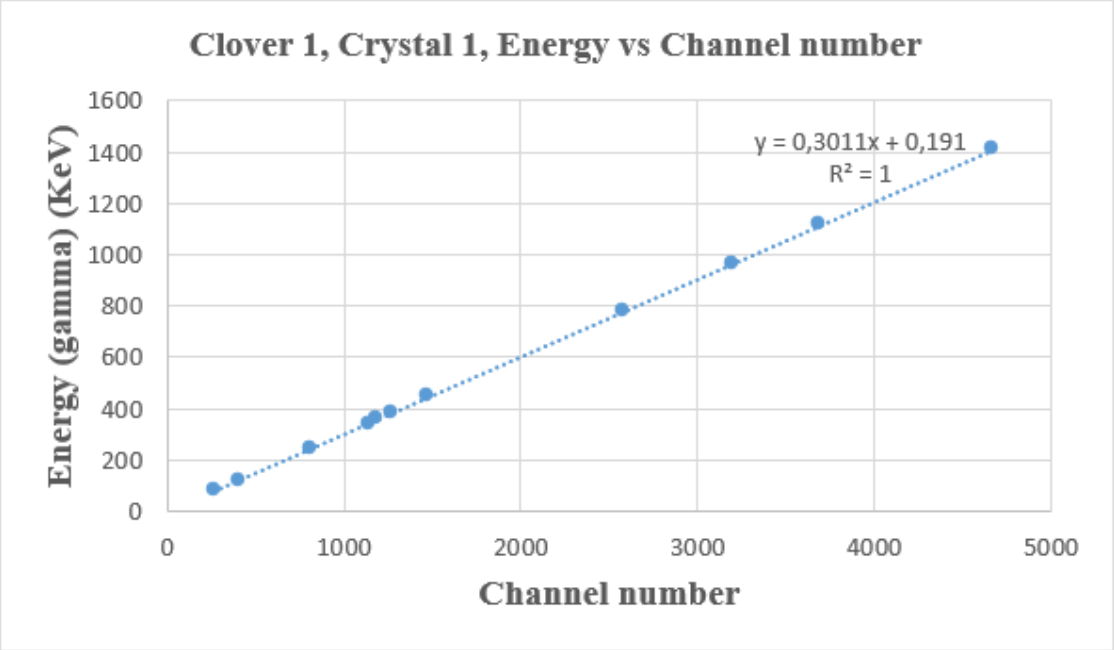

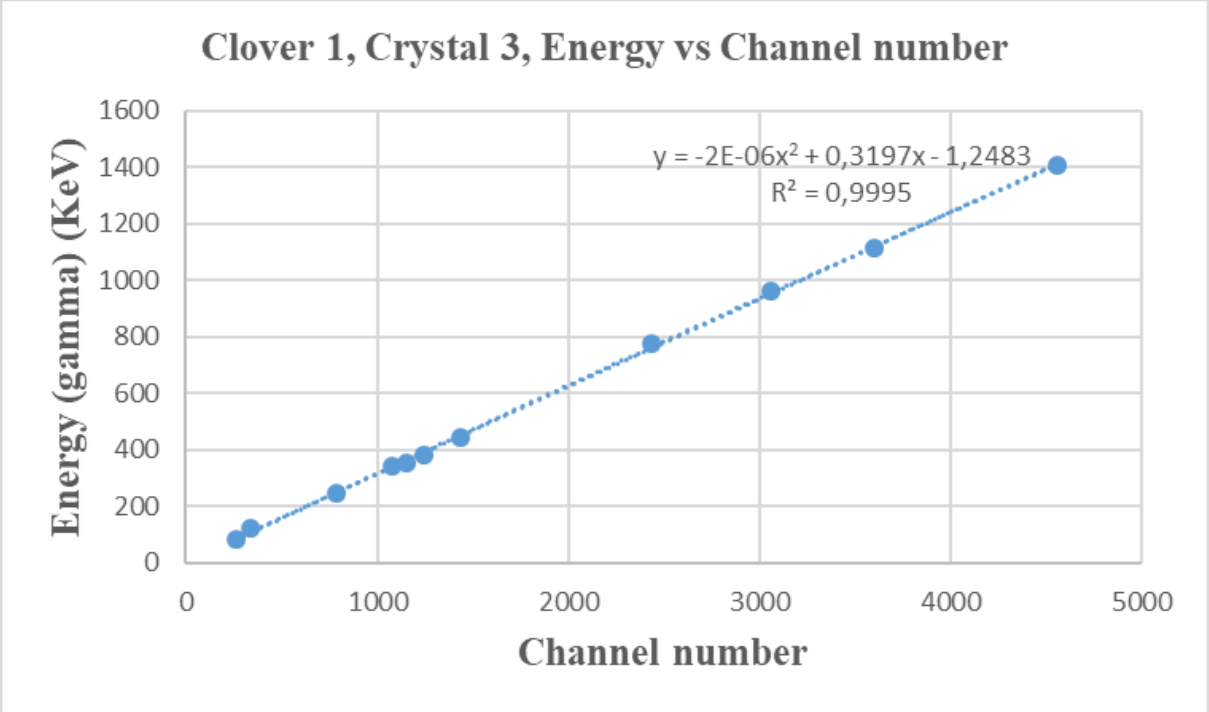

Figure 22: Energy calibration of Clover 1, Crystal 3 using a linear and quadratic fit function

Source	Channel Number	Energy (gamma) (keV)	Calculated (linear)	Calculated (quadratic)	Residual (linear)	Residual (quadratic)
^{133}Ba	261	80.999	86.8779	82.0572	5.8789	1.0582
^{152}Eu	342	121.783	111.9393	107.8552	-9.8437	-13.9278
^{152}Eu	791	244.692	250.8599	250.3831	6.1679	5.6910
^{152}Eu	1077	344.276	339.3483	340.7487	-4.9277	-3.5273
^{133}Ba	1152	356.010	362.5533	364.3919	6.5433	8.3819
^{133}Ba	1242	383.860	390.3993	392.7339	6.5393	8.8739
^{152}Eu	1436	443.976	450.4229	453.7167	6.4469	9.7407
^{152}Eu	2432	778.903	758.5853	764.4329	-20.3177	-14.4701
^{152}Eu	3059	964.131	952.5791	957.9900	-11.5519	-6.1320
^{152}Eu	3598	1112.116	1119.3457	1123.1411	7.2297	11.0251
^{152}Eu	4557	1408.011	1416.0603	1414.0921	8.0493	6.0811

Table 4: Gamma energy data with linear and quadratic calculations and residuals for Clover 1, Crystal 3

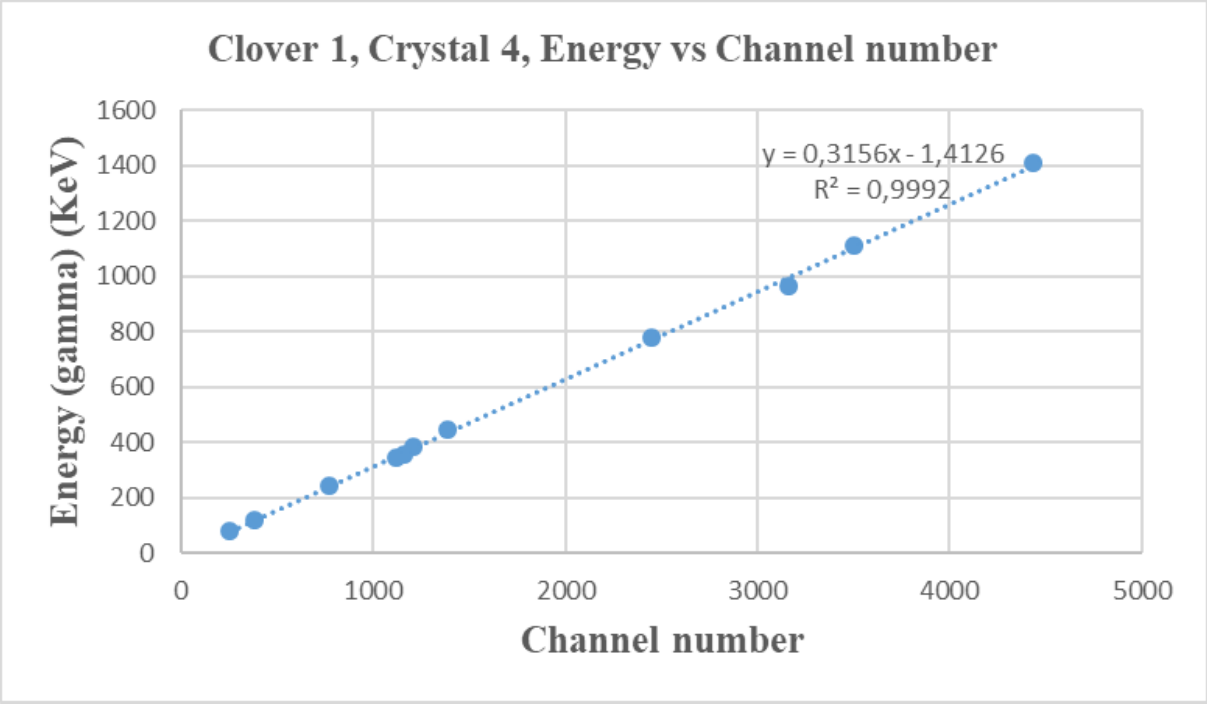

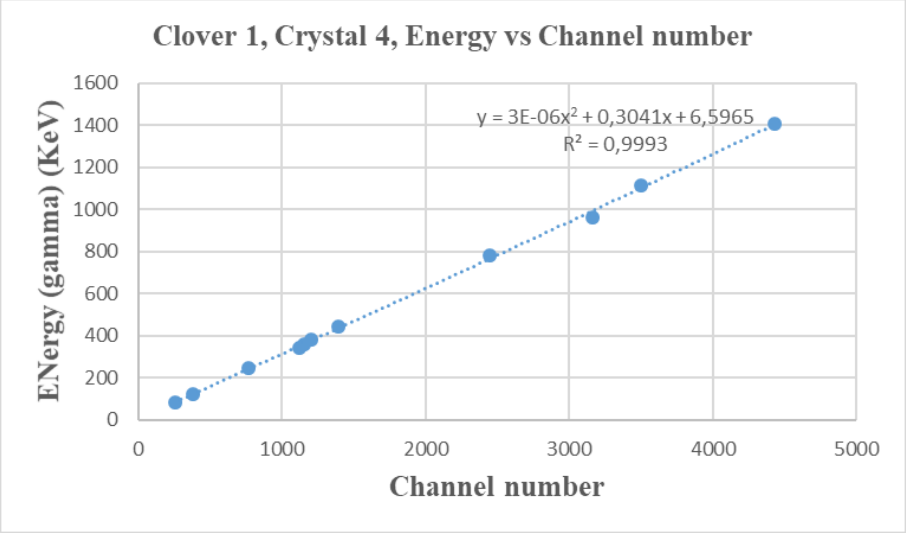

Figure 23: Energy calibration of Clover 1, Crystal 4 using a linear and quadratic fit function

Source	Channel Number	Energy (gamma) (keV)	Calculated (linear)	Calculated (quadratic)	Residual (linear)	Residual (quadratic)
^{133}Ba	254	80.999	78.7498	84.031448	-2.2492	3.032448
^{152}Eu	383	121.783	119.4622	123.506867	-2.3208	1.723867
^{152}Eu	769	244.692	241.2838	242.223483	-3.4082	-2.468517
^{152}Eu	1119	344.276	351.7438	350.640883	7.4678	6.364883
^{133}Ba	1156	356.01	363.421	362.145108	7.411	6.135108
^{133}Ba	1207	383.86	379.5166	378.015747	-4.3434	-5.844253
^{152}Eu	1390	443.976	437.2714	435.0918	-6.7046	-8.8842
^{152}Eu	2449	778.903	771.4918	769.330203	-7.4112	-9.572797
^{152}Eu	3163	964.131	996.8302	998.478507	32.6992	34.347507
^{152}Eu	3499	1112.116	1102.8718	1107.371403	-9.2442	-4.744597
^{152}Eu	4431	1408.011	1397.011	1412.964883	-11	4.953883

Table 5: Gamma energy data with linear and quadratic calculations and residuals for Clover 1, Crystal 4

Clover 1	**Linear Fit Coefficients** $(y = kx + b)$		**Quadratic Fit Coefficients** $(y = ax^2 + bx + c)$		
	k	**b**	**a**	**b**	**c**
Crystal 1	0.3011	0.1910	$-7 \cdot 10^{-6}$	0.3014	-0.0432
Crystal 2	0.2913	14.2130	$8 \cdot 10^{-6}$	0.2530	41.1830
Crystal 3	0.3094	6.1245	$-2 \cdot 10^{-6}$	0.3197	-1.2483
Crystal 4	0.3156	-1.4126	$3 \cdot 10^{-6}$	0.3041	6.5965

Table 6: Coefficients for linear and quadratic fits for Clover 1 crystals

Spectrums of calibrated detector crystals

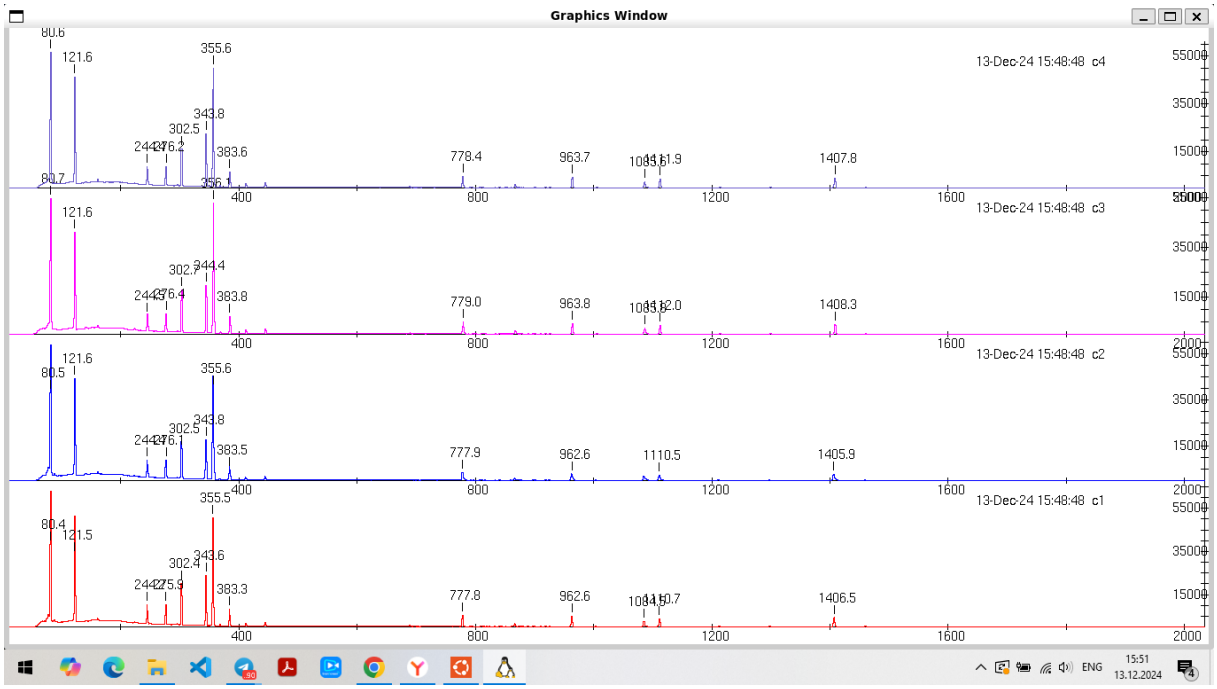

Figure 24: Calibrated spectra for Clover 1

Isotope	Energy (Gamma)	Error	Channel Number	Error	Area	Error	Width	Error
^{133}Ba	80.9990	0.004	268	19	117121	342	4.11	4
^{152}Eu	121.7830	0.002	405	14	94095	306	4.43	3
^{152}Eu	244.6920	0.002	812	4	17462	132	4.65	9
^{152}Eu	344.2760	0.004	1143	31	48752	220	5.16	3
^{133}Ba	356.0100	0.009	1182	5	120288	346	4.89	7
^{133}Ba	383.8600	0.009	1274	22	16147	127	5.30	3
^{152}Eu	443.9760	0.005	1474	3	4398	66	5.43	8
^{152}Eu	778.9030	0.006	2586	3	11939	109	6.11	8
^{152}Eu	964.1310	0.009	3201	4	11641	107	6.47	11
^{152}Eu	1112.1160	0.70	3693	13	9556	97	6.68	21
^{152}Eu	1408.0110	0.014	4677	18	12480	112	7.91	20

Table 7: Energy calibration data for ^{152}Eu and ^{133}Ba for Clover 1, Crystal 1.

Isotope	Energy (Gamma)	Error	Channel Number	Error	Area	Error	Width	Error
^{133}Ba	80.9990	0.004	216	6	113210	336	4.41	24
^{152}Eu	121.7830	0.002	285	16	328198	572	5.212	22
^{152}Eu	244.6920	0.002	598	5	16110	126	6.18	6
^{152}Eu	344.2760	0.004	1125	3	43805	220	7.26	4

^{133}Ba	356.0100	0.009	1164	4	110136	331	7.541	24
^{133}Ba	383.8600	0.009	1257	6	11487	107	8.10	9
^{152}Eu	443.9760	0.005	1454	2	3850	62	9.41	17
^{152}Eu	778.9030	0.006	2761	3	526	72	13.06	21
^{152}Eu	964.1310	0.009	3293	5	782	27	14.74	20
^{152}Eu	1112.1160	0.700	3832	6	1500	32	15.9	3
^{152}Eu	1408.0110	0.014	4645	68	4068	23	22.5	23

Table 8: Energy calibration data for ^{152}Eu and ^{133}Ba for Clover 1, Crystal 2.

Isotope	**Energy (Gamma)**	**Error**	**Channel Number**	**Error**	**Area**	**Error**	**Width**	**Error**
^{133}Ba	80.9990	0.004	261	8	110545	332	4.89	10
^{152}Eu	121.7830	0.002	342	18	165729	407	5.401	21
^{152}Eu	244.6920	0.002	791	9	16172	127	5.40	11
^{152}Eu	344.2760	0.004	1077	32	89826	299	5.79	3
^{133}Ba	356.0100	0.004	1152	9	15118	336	5.82	3
^{133}Ba	383.8600	0.009	1242	3	15118	122	5.94	4
^{152}Eu	443.9760	0.005	1436	7	4164	64	5.5	5
^{152}Eu	778.9030	0.006	2432	49	81391	285	6.79	10
^{152}Eu	964.1310	0.006	3059	25	11357	207	7.22	8
^{152}Eu	1112.1160	0.007	3598	59	9494	220	7.3	5
^{152}Eu	1408.0110	0.014	4557	90	11025	110	7.7	13

Table 9: Energy calibration data for ^{152}Eu and ^{133}Ba for Clover 1, Crystal 3.

Isotope	**Energy (Gamma)**	**Error**	**Channel Number**	**Error**	**Area**	**Error**	**Width**	**Error**
^{133}Ba	80.9990	0.004	254	15	10989	330	4.36	6
^{152}Eu	121.7830	0.002	383	10	88491	297	4.904	23
^{152}Eu	244.6920	0.002	769	24	17270	131	5.00	9
^{152}Eu	344.2760	0.004	1119	17	51513	336	5.31	12
^{133}Ba	356.0100	0.004	1155	5	10395	105	5.5	7
^{133}Ba	383.8600	0.009	1207	3	15205	155	5.50	5
^{152}Eu	443.9760	0.005	1431	37	5237	72	5.65	19
^{152}Eu	778.9030	0.006	2449	50	500	85	6.3	12
^{152}Eu	964.1310	0.006	3499	44	100	44	6.3	3
^{152}Eu	1408.0110	0.014	4431	111	12356	111	7.3	22

Table 10: Energy calibration data for ^{152}Eu and ^{133}Ba for Clover 1, Crystal 4.

Requirement of detector calibration

Why do we need to calibrate the detector before an experiment?

Calibration is essential in spectroscopic detectors to ensure that the channel numbers on the x-axis accurately correspond to the true energy of the detected photons or particles. Calibration of detectors before conducting an experiment is a critical step to ensure the accuracy and reliability of the measurements.Calibrating detectors before an experiment is vital to ensure accurate, consistent, and reliable measurements. By correcting for variations, environmental effects, and detector-specific issues, calibration enables precise data collection and interpretation. Without it, the experiment's results may be unreliable or invalid.Below are the key reasons why calibration is necessary:

1. **Conversion from ADC Channels to Energy:** Detectors measure energy deposition in a medium, but the raw output is typically in analog-to-digital converter (ADC) channels. Calibration converts these channel numbers into physical energy values (e.g., keV or MeV) using a known relationship between channel numbers and energy.
2. **Systematic Variations:** Variations in electronic response, crystal geometry, or even detector aging can cause deviations in the recorded channel numbers for a given energy. Calibration accounts for these effects.
3. **Comparison with Known Standards:** Calibration allows experimental results to be compared against theoretical predictions, databases, or other experimental results.
4. **Accuracy in Quantitative Analysis:** Without calibration, peak positions may be misinterpreted, leading to errors in identifying isotopes, determining activity, or conducting other quantitative measurements.

Detector calibration is essential to ensure accurate, consistent, and reliable measurements in experiments. Calibration accounts for variations between different detectors, compensates for environmental influences, ensures correct peak identification, and optimizes data quality. It also adjusts for aging, wear, and degradation of the detector over time, ensuring consistent performance. Additionally, calibration provides a standardized response across multiple detectors, making it possible to compare results from different systems. Finally, it enables reliable quantitative analysis, ensuring that the recorded data reflects the true physical processes being studied.

6.Summary of project

Through the present work, a detailed study of the prompt gamma-ray interaction mechanisms has been performed. The theoretical Klein-Nishina cross-section relation was derived and simulated using a C code. The simulation code was developed to describe the differential cross-section for Compton scattering of photons with four different energies. The discussions further revealed the importance of semiconductor detectors in the field of gamma-ray spectroscopy. This is due to the ever-increasing demand for better energy resolution and high efficiency. All these features can be optimally achieved with HPGe Clover detectors. Clover detectors, with their excellent resolution, enhanced photopeak efficiency, high peak-to-total ratio through addback, and Compton suppression, are crucial in building complex level schemes and deducing the nuclear structure of exotic nuclides. Their compact nature makes them ideal for applications such as soil characterization, radiation monitoring, and more. Large arrays of gamma detectors, such as Gammasphere, which comprises different types of segmented HPGe detectors, hold the future of gamma-ray spectroscopy measurement techniques across the globe.Radware software is used in nuclear physics for processing and analyzing data obtained through gamma-ray spectroscopy. Radware is used for spectrum processing, calibration, peak identification, and spectral analysis.

Gamma-ray spectroscopy is a method of analysis based on studying gamma radiation emitted by radioactive materials. In this project, we used a Clover detector, which measured the energy and intensity of gamma rays emitted by the standard radioactive sources ^{133}Ba and ^{152}Eu were used. The nuclear level schemes were prepared using the GLS code from the RADWARE software package.

The gamma-rays from ^{133}Ba and ^{152}Eu were collected using an n-type Clover detector. The Clover detector was maintained at liquid nitrogen temperature by pressure filling the dewar. The Clover detector is composed of four closely packed n-type Hyper-Pure Germanium (HPGe) crystals. The gamma-ray spectrum was obtained from each crystal of the Clover detector in `.spe` format. The photopeaks corresponding to different prompt gamma-ray transitions from the two sources were fitted using the RADWARE software. The fitting algorithm from the program code `GF3` was utilized to find the centroid of the photopeaks in channel numbers. The individual Clover crystals were calibrated using linear and quadratic functions. Based on the fitting functions, the residuals were calculated corresponding to both the linear and quadratic fits. The spectrum was then calibrated using the coefficients from the quadratic fit. Therefore, the calibration of the Clover detector was properly performed.

References

[1] P.J. Nolan, Nucl. Phys. A. 520 (1990) 657c.

[2] G. F. Knoll, Radiation Detection and Measurement (3rd edition), John Wiley and Sons, United States of America (2000).

[3] Advanced laboratory, Physics 407 (Revised 4/27/01). Madison, WI: University of Wisconsin.

[4] Khater, A. (2006). Radiation detection methods. In [Editor(s) if available], Title of the book (pp. 100-120). Publisher.Springer.

[5] Podgorsak, E. B. (Ed.). (2016). Radiation oncology physics: A handbook for teachers and students.

[6] Knoll, G. F. (2014). Radiation detection and measurement (4th ed.). Wiley.

[7] G. Gilmore, J. Hemingway, Practical Gamma-Ray Spectrometry, John Wiley & Sons, 1995.

[8] W.R. Leo, Techniques for Nuclear and Particle Physics Experiments, SpringerVerlag, 1987.

[9] National Institute of Standards and Technology, X-Ray Mass Attenuation Coefficients, https://physics.nist.gov/PhysRefData/XrayMassCoef/tab3.html, accessed: 12.07.2018.

[10] Joshi, P. K., Jain, H. C., Medhi, A. S., Chattopadhyay, S., Bhattacharya, S., Goswami, A. (1997). Study of the characteristics of a clover detector. Nuclear Instruments and Methods in Physics Research A, 399, 51-56. https://doi.org/10.1016/S0168-9002(97)00493-4

[11] Mirion Technologies, Inc. (2017). Copyright notice. Mirion Technologies (Canberra), Inc. Retrieved from https://www.mirion.com https://www.mirion.com

[12] Radware, David Radford's RadWare nuclear physics data analysis software. https://github.com/radforddc/rw05/tree/main